New Constraints on Early Mars Weathering Conditions From an Experimental Approach on Crust Simulants

Fabien Baron, A. Gaudin, J.-P Lorand, N. Mangold

JGR Planets

RESEARCH ARTICLE
10.1029/2019JE005920

New Constraints on Early Mars Weathering Conditions From an Experimental Approach on Crust Simulants

F. Baron[1], A. Gaudin[1], J.-P. Lorand[1], and N. Mangold[1]

[1]LPG UMR 6112 CNRS/Université de Nantes, Nantes, France

Key Points:
- Chemical weathering in mildly acidic conditions under a CO_2 atmosphere yielded leaching of alkali and alkaline earth elements
- Mass balance calculations indicated Al, Fe, and Si enrichment in the weathering products
- Our results imply unsuitable conditions for carbonate formation despite CO_2 in the Martian atmosphere

Supporting Information:
- Supporting Information S1

Correspondence to:
F. Baron,
fabien.baron@univ-nantes.fr

Citation:
Baron, F., Gaudin, A., Lorand, J.-P., & Mangold, N. (2019). New constraints on early Mars weathering conditions from an experimental approach on crust simulants. *Journal of Geophysical Research: Planets*, *124*, 1783–1801. https://doi.org/10.1029/2019JE005920

Received 14 JAN 2019
Accepted 19 MAY 2019
Accepted article online 30 MAY 2019
Published online 10 JUL 2019

Abstract A denser CO_2 atmosphere and higher temperatures than present-day conditions are frequently invoked as prevailing conditions for the formation of some ancient hydrous mineralogical associations present at the surface of Mars. The environmental conditions are of particular interest to better understand and constrain the weathering processes of the early Martian crust. For this purpose, 6-month-long batch weathering experiments on Martian crust simulants and individual Martian mineral analogs were performed at low temperature (45 °C) under a dense CO_2 atmosphere (1 atm). Constraints on the weathering conditions are deduced from the solution properties and thermodynamic calculations, as well as mass balance calculations. Experimental solutions vary from mildly acidic to near neutral (4.75–6.48 pH). The Eh-pH conditions (Eh from 0.189–0.416 V/standard hydrogen electrode) suggest favorable conditions for the formation of ferric minerals despite an anoxic CO_2 atmosphere. The chemical weathering appears to be 4 times more intense for Martian simulants under a CO_2 atmosphere than under Earth ambient air. The weathering trend under a CO_2 atmosphere involves leaching of alkali and alkaline earth elements (Mg, Ca, Na, and K) and Si and enrichments of the solid phases in Al, Fe, and to a lesser extent Si compared to the initial chemical composition of the starting minerals. This geochemical partitioning between solution and solids resembles those deduced from weathering profiles on Earth. Our results strongly support the idea that carbonates could not have extensively formed at the surface of early Mars despite a dense CO_2 atmosphere.

Plain Language Summary Mars orbital and landed missions have provided mineralogical, morphological, and field evidence for liquid water at the surface approximately 3.5 billion years ago. The chemical and mineralogical composition of the Martian rocks have potentially been modified by interaction with this liquid water. The purpose of our study is to use laboratory experiments to constrain the physicochemical conditions of water resulting from the chemical weathering of Martian crust simulants under an atmosphere composed of carbon dioxide, as is the case for Mars. The water in contact with simulants is mildly acidic. The partitioning of chemical elements between the solution and minerals is similar to what is observed on Earth, but weathering is more intense. Despite that Mars had a primitive CO_2-dense atmosphere, the conditions were not favorable to the extensive formation of carbonate at the surface.

1. Introduction

Extensive networks of fluvial valleys (e.g., Achille & Hynek, 2010; Ansan et al., 2011; Craddock & Howard, 2002), strongly degraded impact craters (Craddock et al., 1997; Mangold et al., 2012), and the presence of fluvial and lacustrine sediments (e.g., Grotzinger et al., 2014, 2015; Mangold et al., 2016) argue in concert for at least episodic presence of an active hydrosphere on early Mars at ca. 3.5–3.8 Ga. In addition, the orbital and in situ characterization of hydrated/hydroxylated mineral associations such as clay minerals (mainly Fe-Mg clay minerals), hydrated sulfates, Fe-[(oxy)hydr]oxides, and local carbonates provide a separate set of evidence for widespread surface fluid-rock interactions on early Mars (e.g., Bibring et al., 2005, 2006; Bristow et al., 2018; Carter et al., 2013, 2015; Ehlmann et al., 2013; Mangold et al., 2019; Poulet et al., 2005; Vaniman et al., 2014).

The Mars Atmosphere and Volatile EvolutioN (MAVEN) observation of the Mars upper atmosphere allowed to determine the actual loss rates of H and O, thus suggesting that a major fraction of the atmosphere was lost to space very early in the history of Mars (Jakosky et al., 2018), perhaps as early as 4.4 Ga according to hydrogen isotope compositions of prenoachian lithologies of regolith breccia meteorite NWA 7533 (Nemchin et al., 2014). The extrapolation of these loss rates over the history of the planet indicates a likely lower limit for the total atmospheric escape of approximately 0.8 bar CO_2 or a 23 m global equivalent layer of

H_2O (Jakosky et al., 2018). These lower estimations of the total atmospheric escape coupled with the observations of the Martian surface argue for potentially intense fluid-rock interactions under an ancient Martian atmosphere dominated by CO_2.

Numerical chemical models have been used to investigate the formation conditions of hydrous/hydroxylated mineralogy under a dense CO_2 atmosphere but failed to reproduce the mineralogy observed at the Martian surface (Zolotov & Mironenko, 2016). Long-term laboratory experiments are useful to better understand near-surface fluid-rock interactions at low temperature by controlling the weathering conditions and the mineralogy of the initial material. Indeed, in this context of low temperature, all reactions are largely controlled by kinetics and surface energy, which greatly complicate any modeling of such systems. Several weathering experiments were conducted with a better understanding of the prerequisite chemical conditions leading to the formation of the identified hydrous/hydroxylated mineralogy observed at the Martian surface by in situ and orbital observations. These previous studies, however, favored high temperatures (>190 °C) that cannot represent surface conditions (Peretyazhko et al., 2016, 2018; Schröder et al., 2004) and/or highly acidic conditions (≤pH 4) relevant for local early Martian environments (Chevrier et al., 2004; Dehouck et al., 2012; Marcucci & Hynek, 2014; Peretyazhko et al., 2018; Tosca et al., 2004). Only Dehouck et al. (2014) and Gaudin et al. (2018) performed experimental weathering closer to presumed surface conditions. However, their experiments were based on a highly magnesian olivine (Fo_{92}), which does not reflect the actual mineralogy of the early Martian crust, where a greater amount of alkali feldspars than previously assumed was deduced from in situ analyses by the *Curiosity* rover and recent studies on paired samples of regolith impact breccia meteorites (Agee et al., 2013; Hewins et al., 2017; Humayun et al., 2013; McCubbin et al., 2016; Morrison et al., 2018; Sautter et al., 2015; Wittmann et al., 2015). Consequently, the geochemical conditions of solutions such as acidity, redox conditions, alkalinity, and chemical composition generated by the weathering process of a more felsic Martian crust on early Mars are still far from fully understood.

To address this long list of questions, we performed weathering experiments on single rock-forming minerals and on Martian crust simulants of alkali basaltic or andesite basaltic composition under low-temperature conditions and a dense CO_2 atmosphere. The present paper reports the chemical properties of experimental solutions to determine the geochemical conditions that could have occurred during a weathering process at the surface of early Mars. The full characterization of the weathering products will be addressed in a forthcoming paper. Thermodynamic calculations were performed from the experimental solutions to constrain some physicochemical properties and to calculate the saturation indices of minerals. Mass balance calculations were also conducted to constrain the chemical composition of weathering products and to determine the potential weathering trend that may have been produced on the early Martian surface.

2. Materials and Methods

2.1. Starting Materials

The mineralogy of the early Martian crust and crystal chemistry of its constituent minerals were first determined from orbital data, yielding a predominantly feldspar-poor pyroxene-dominated mafic crust in ancient highlands (Bandfield, 2002; Mustard et al., 2005; Poulet et al., 2009). This putative crust composition was recently improved by in situ analyses with the CheMin and ChemCam instruments onboard the *Curiosity* rover operating in Gale crater (e.g., Morrison et al., 2018; Sautter et al., 2015) and petrochemical studies of Martian regolith breccia meteorites that had sampled impact lithologies of the early Martian crust (i.e., the paired stones NWA 7533, NWA 7475, and NWA 7034; Agee et al., 2013; Hewins et al., 2017; Humayun et al., 2013; McCubbin et al., 2016; Wittmann et al., 2015). As major results, these studies pointed to more felsic and alkaline-rich mineral assemblages than previously thought. This results was highlighted by the identification of abundant potassium (K) feldspar in both data sets (Hewins et al., 2017; Humayun et al., 2013; Sautter et al., 2015). Thanks to these recent advances, we are able to prepare synthetic Martian crust simulants with a more realistic composition for the early Martian crust compared to previous experiments.

Eight terrestrial mineral species were selected as starting material; a ferroan olivine (Fo_{65}; Bushveld complex, South Africa), a magnesian olivine (Fo_{92}; San Carlos, New Mexico, USA), orthopyroxene (En_{85}; Bushveld complex, South Africa), clinopyroxene (augite; Massif central, France), plagioclase (An_{60};

Table 1
Mineral Modal Compositions of the Two Martian Crust Simulants

Mineral	Martian simulant (O) (wt.%)	Martian simulant (M) (wt.%)
Ferroan olivine (Fo_{65})	11.8	0.0
Orthopyroxene (En_{80})	17.7	17.8
Clinopyroxene (augite)	23.5	23.7
Plagioclase (An_{60})	32.4	32.7
K-feldspar (Or_{85})	12.8	12.9
Magnetite	0.0	10.9
Apatite	2.0	2.0

unknown origin), K-feldspar (Or_{85}; Eifel volcanism, Germany), apatite (Durango, Mexico), and magnetite (El Romeral mine, Chile). These starting minerals were selected because they show close compositional similarities with the early Martian crustal mineralogy described in Gale crater (Morrison et al., 2018) and in the Martian regolith breccia NWA 7533 (Hewins et al., 2017; see Table S1). Their geological settings and providers are reported in the supporting information (Text S1). Each starting mineral was analyzed at the Institut des Matériaux de Nantes on a polished section using a scanning electron microscope (SEM) equipped with an energy dispersive spectrometer (Table S2; more details on the analytical procedure are presented in Text S2).

Each starting mineral was first crushed in an agate mortar and then sieved to obtain a 160- to 1,000 μm size fraction. Each grain of mineral was then handpicked under a binocular microscope to remove as many visible impurities as possible. The remaining fraction was then crushed again in an agate mortar and sieved to obtain a <63 μm size fraction. Magnetic particles were removed from the samples using a hand magnet. The <63 μm size fraction for each mineral was then washed in ethanol using an ultrasonic gun to prevent any incipient alteration and to sterilize the starting materials. During this step, the <2 μm fraction was also removed using sedimentation in ethanol to prevent the presence of secondary silicate minerals (e.g., clay minerals and amorphous materials) already present in the starting materials.

The purity of starting minerals (2- to 63 μm fraction) was checked at the Institut des Matériaux de Nantes by X-ray diffraction (Figure S1). The high purity of Mg-olivine (Fo_{92}) was already evidenced by Dehouck et al. (2014) on the <63-μm fraction following the same preparation procedure. Apatite was not analyzed due to its gem quality. A calcic plagioclase was identified in very low amounts (close to the detection limit) in the orthopyroxene (Figure S1). Apatite was also identified in the magnetite. An additional check for secondary minerals (e.g., clay minerals and carbonates) in the starting materials (2- to 63 μm fraction) was performed using reflectance near-infrared spectroscopy and transmission midinfrared spectroscopy (LPG Nantes). This method detected only a minor amount of talc in the orthopyroxene. No evolution of the talc content was observed after the weathering experiments on orthopyroxene.

2.2. Martian Crust Simulants

Two early Martian crust simulants were prepared to fit the mineralogical assemblages and the compositional ranges documented by the Martian regolith breccia meteorites (Tables 1–3; Agee et al., 2013; Hewins et al., 2017; Humayun et al., 2013; Wittmann et al., 2015; Taylor & McLennan, 2009). One simulant comprises ferroan olivine (Fo_{65}; named Martian simulant (O) throughout this paper). The second simulant (named Martian simulant (M) throughout this paper) was prepared with magnetite instead of ferroan olivine. In detail, these two Martian simulants were prepared by mixing the 2- to 63 μm fractions of each of the starting minerals. The resulting modal proportions are presented in Table 1. The chemical compositions of the Martian simulants were calculated from the chemical compositions of the starting minerals (Table 3). The high proportion of feldspars and the relatively low Fe content of both pyroxenes account for the relatively low Fe content of simulant (O) compared to that of Martian rocks (Tables 1 and 2). The Martian simulant (M) reproduces the near-zero olivine content of regolith breccia meteorites and better fits with the high Fe content of Martian rocks (Table 3). The high proportion of K-feldspar in both Martian crust simulants compensates the low Na-content of plagioclase (An_{60}) for fitting the total alkali content (Na and K) of the Martian regolith breccia meteorites (Tables 2 and 3). In a total alkali silica (TAS) diagram (Le Bas et al., 1986), simulant (O) plots within the compositional field of basaltic andesite, whereas simulant (M) corresponds to basaltic compositions. These two Martian crust simulants were newly prepared for each weathering experiment to obtain the same mineral proportions between each experimental run. The errors in the weighing of each constituent of simulants were less than 0.2 wt.%.

Table 2
Mineral Modal Compositions of the Martian Breccia Meteorites NWA 7034 and NWA 7533

Mineral	NWA 7034 (wt.%)	NWA 7533 (wt.%)
Olivine	0	0
Orthopyroxene	25.4	47.2
Clinopyroxene	18.2	
Plagioclase	38.0	33.5
K-feldspar	4.9	2.6
Iron oxides	9.7	13.5
Apatite	3.7	3.2

Note. The mineralogical compositions of the impact breccia meteorites (NWA 7034 and NWA 7533) were taken from Agee et al. (2013) and Hewins et al. ((2013)), respectively.

Table 3
Calculated Bulk Chemical Compositions of Martian Rock Simulants

	Martian simulant (O) wt.%	Martian simulant (M) wt.%	Mars Upper Crust[a] wt.%	NWA 7034[a] wt.%	NWA 7475[a] wt.%
SiO_2	52.5	49.3	50.2	50.9	49.2
Al_2O_3	13.3	13.7	10.7	12.0	10.9
FeO	6.9	12.9	18.5	13.9	16.9
MgO	13.2	9.6	9.2	8.4	11.1
CaO	8.4	8.6	7.0	9.6	7.2
Na_2O	2.0	2.1	3.0	4.0	2.9
K_2O	1.9	2.0	0.5	0.4	0.5
P_2O_5	1.7	1.8	0.9	0.8	1.3
Σ	100	100	100	100	100

Note. Chemical compositions of Martian crust simulants calculated from the structural formulas of starting minerals.
[a]Chemical compositions of the impact breccia meteorites and Mars upper crust after Agee et al. (2013), Wittmann et al. (2015), and Taylor and McLennan (2009), respectively.

2.3. Experimental Setup

The procedure chosen to reproduce surface weathering processes dominated by the Martian atmospheric conditions involved a closed system (without exchanges of matter with its environment) and a relatively low water/rock ratio. These weathering experiments are the best way to reproduce natural environments of microsystems that operate during the earliest stages of weathering in nature (i.e., near the alteration front; Velde & Meunier, 2008, and references therein).

Weathering experiments were performed at the LPG (Nantes) under simulated early Mars surface conditions (anoxic conditions). These experiments were carried out on both individual minerals and synthetic Martian crust simulants. For comparison, the same series of experiments was carried out under terrestrial atmospheric conditions (ambient air). Anoxic experiments were performed under 1 atm of CO_2 (Air Liquide® Alphagaz CO_2) in a Mbraun-LABstar glovebox. The concentration of O_2 inside the glovebox was continuously controlled using an electrochemical oxygen analyzer (MB-OX-EC-PLC, over the 1- to 1000 ppm range). The partial pressure of oxygen (pO_2) in the glovebox was below 5×10^{-8} atm (<0.5 ppm) during the experiments thanks to a gas purification unit.

The experiments were performed at 45 °C (thermostatic hot plate) for 6 months. This temperature of 45 °C was chosen to increase the reaction rate without modifying the reaction pathway compared to room temperature, as shown previously by Dehouck et al. (2014) and Dehouck et al. (2016). Briefly, 1.8 g of starting materials (minerals or simulants) and 18 mL of Milli-Q® ultrapure water (18 MΩ cm) were introduced into batch Savillex™ PFA reactors (90 mL) under continuous stirring (50 rpm using an orbital agitator). Milli-Q® ultrapure water (18 MΩ cm) was previously degassed under vacuum for anoxic experiments and then equilibrated under continuous stirring for 2 days with 1 atm of CO_2 or terrestrial ambient air for the anoxic or oxic experiments, respectively. The reactors remained closed during all the experiments. Possible leaks during the experiments were checked by controlling the weight of reactors during the whole duration of the experiments. The average leak corresponded to 0.17 (±0.1) ml of solution for 6 months. For each starting mineral or Martian crust simulant, only one weathering experiment was performed due to the time-consuming preparation for obtaining requested amount of the pure starting minerals.

2.4. Physicochemical Properties of Experimental Solutions

Eh (±2.5 mV) and pH (±0.05) values for ultrapure water in equilibrium with ambient air or CO_2 atmosphere were measured at 25 °C after equilibration under continuous stirring for 2 days and before any contact with individual minerals or simulants.

At the end of the experiments, the pH and the Eh values of each experimental solution were measured in contact with minerals at 25 °C (Table S3). These measurements were performed 1 hr after the end of weathering runs when the temperature inside reactors had decreased to that of the room or the glovebox (25 °C; more details in Text S3).

Total concentrations of major cations (Si, Al, Fe, Mg, Ca, K, and Na) in <0.2μm filtrated solutions were measured (Table S3) using inductively coupled plasma atomic emission spectroscopy (ICP-AES; LPG, Nantes; more details in Texts S3 and S4). Total dissolved carbon was not measured because CO_2 in the solution quickly reequilibrated with respect to the glovebox or ambient atmosphere after the opening of reactors. This concentration was estimated for each experimental solution from thermodynamic calculations of the aqueous speciation of elements at 25 °C (Table S3 and see details in Text S5). The total dissolved carbon was estimated by assuming the electroneutrality of the solution. The calculations were performed using the PHREEQC® software (Parkhurst & Appelo, 2013) associated with the Thermoddem database (http://thermoddem.brgm.fr/). The pH values were also estimated at 45 °C (Tables 4 and S3) using the same procedure. From this aqueous speciation of elements at 45 °C, Eh-pH diagrams were constructed for each experimental solution using the Chess© software (van der Lee, 1998) associated with the Thermoddem database

Table 4
Table of pH, Eh, and Relative Abundances of Dissolved Elements in Experimental Solutions Under Ambient Air and CO_2 Atmosphere

Atmosphere	Starting Material	Eh (V/SHE)	pH (45 °C)	Elements in solution
Air	Mg-olivine (Fo_{92})	0.410	8.05	Mg
	Ferroan olivine (Fo_{65})	0.431	7.70	Mg > Si
	Clinopyroxene (augite)	0.434	7.60	Si > Ca
	Orthopyroxene (En_{80})	0.443	7.45	Si > Ca > Mg > K
	Plagioclase (An_{60})	0.462	6.63	Si > Ca > Na > K > Al > Mg
	K-Feldspar (Or_{85})	0.477	6.04	Si > K > Na > Al > Ca
	Martian simulant (O)	0.450	7.42	Si > Mg > Ca > K
	Martian simulant (M)	0.465	7.08	Si > Ca > Mg > K
CO_2	Mg-olivine (Fo_{92})	0.228	6.42	Mg > Si > Fe
	Ferroan olivine (Fo_{65})	0.189	6.48	Mg > Si > Fe
	Clinopyroxene (augite)	0.318	5.92	Ca > Mg > Si
	Orthopyroxene (En_{80})	0.241	6.30	Mg > Si > Ca > K
	Plagioclase (An_{60})	0.347	5.55	Ca > Si > Na > K > Al > Mg > Fe
	K-Feldspar (Or_{85})	0.416	4.75	Si > K > Na > Al > Ca > Fe > Mg
	Martian simulant (O)	0.304	5.69	Ca > Si > Mg > Na > K
	Martian simulant (M)	0.299	5.58	Si > Ca > Mg > Na > Fe > K

(http://thermoddem.brgm.fr/). Each diagram was calculated using the chemical composition of solutions presented in Table S3.

2.5. Estimated Compositions of the Weathering Products

Silicate weathering commonly produces a hydrated surface layer (amorphous and crystalline phases) at the mineral-solution interface under a wide range of pH values and temperatures (e.g., Banfield & Eggleton, 1990; Daval et al., 2011; Nesbitt & Muir, 1988; Nugent et al., 1998; Putnis, 2014; Ruiz-Agudo et al., 2012; Ruiz-Agudo et al., 2016; Zhu et al., 2006). At low temperatures, however, weathering experiments are known to produce only very small amounts of weathering products (see Figures S2 and S3). Thus, these small-sized weathering products can be accurately identified and characterized only with microscale/nanoscale imaging and analytical tools (e.g., transmission electron microscopy or SEM; see Figures S2 and S3) instead of bulk analytical methods (e.g., X-ray diffraction, vibrational spectroscopies, and Mössbauer spectroscopy). However, these micro/nanoscale tools have a major drawback in that they cannot provide data at the bulk sample scale. Consequently, we used a mass balance calculation based on the chemical composition of each experimental solution to estimate the average composition of the weathering products. The calculation started by determining the number of moles of each element dissolved in the experimental solution from the dissolved element concentrations and the volume of the solution. The number of moles of dissolved elements coming from the dissolution of minerals was then calculated from the chemical composition of the starting mineral to account for the chemical composition of the solution. The estimated composition of the weathering products was finally determined by the difference. For the two simulants, the proportion of dissolved mineral is not known for each phase. However, SEM-field emission gun and transmission electron microscopy observations of the grain surfaces revealed that (i) all mineral grains are covered by weathering products, (ii) the amounts of weathering products are very small, and (iii) all mineral grains show the same proportion of dissolution features. Consequently, we assumed that all minerals entering the synthetic composition of both simulants were dissolved at the same rate.

This calculated composition of the weathering products is theoretical and cannot adequately represent the actual composition of the weathering products as a whole. However, it helps greatly in materializing the geochemical weathering trend. The actual chemical composition of the whole weathering products lies somewhere between the estimated composition of the weathering products and the composition of the starting mineralogy.

2.6. Calculation of the Saturation Indices of Minerals

The mineral phases that could precipitate from the solution or could be present in contact with the solution can be determined from thermodynamic equilibrium calculation of the saturation indices of minerals, on the basis of the physicochemical properties of solutions. The saturation indices of minerals were

calculated for each of our experimental solutions from the thermodynamic calculations of the aqueous speciation of elements at 45 °C (PHREEQC® software). For this purpose, the Thermoddem database was implemented with data on additional clay minerals to cover wide a range of chemical compositions as possible for smectite minerals that are not extensively present in the database. The thermodynamic properties of these smectites were estimated using the prediction model of thermodynamic properties of clay minerals developed by Blanc et al. (2015) (Table S4). Minerals that formed at high temperature were not taken into account (Tables S5 and S6). A mineral phase was considered in equilibrium with the solution if its saturation index was between −0.5 and 0.5.

3. Experimental Results

3.1. Eh-pH Properties of Experimental Solutions

Ultrapure water in equilibrium with terrestrial ambient air shows pH and Eh values of 5.3 and 0.415 V/SHE (standard hydrogen electrode), respectively. In contrast, the pH of ultrapure water in equilibrium with 1 atm CO_2 decreases to 3.6, while the Eh value (0.424 V/SHE) is similar under CO_2 or ambient air despite the anoxic atmosphere ($[O_2] < 0.5$ ppm). The low pH value indicates that atmospheric CO_2 is dissolved as aqueous species (e.g., $H_2CO_{3\ (aq)}$).

At the end of the experiments on individual minerals under a CO_2 atmosphere, the pH of the solutions calculated at 45 °C shows a clear evolution controlled by the chemical composition of the starting mineral. Indeed, it decreases from 6.3–6.5 for ferromagnesian minerals (olivines and orthopyroxene) to 5.9 for clinopyroxene and 4.8–5.6 for feldspars (plagioclase and K-feldspar: Table 4). The same trend is observed in the experiments under ambient air in which pH values decrease from 7.5–8.1 for ferromagnesian minerals to 6.0–6.6 for feldspars (Table 4). The high pCO_2 (1 atm) induces a mean decrease of 1.4 pH unit in solutions compared to ambient air (Table 4). The aqueous speciation of dissolved atmospheric CO_2 significantly reduces the variation in pH between ferromagnesian and feldspar minerals under a CO_2 atmosphere. The experimental solutions in contact with Martian simulants show intermediate pH values between those of ferromagnesian minerals and feldspars regardless of the composition of the atmosphere (pH of 5.6 and 5.7 under CO_2 and pH of 7.1 and 7.4 under air). There is no detectable effect of the mineralogical composition of both Martian simulants (i.e., ferroan olivine (Fo_{65}) or magnetite) under a CO_2 atmosphere.

Concerning redox properties under a CO_2 atmosphere, the experiments on individual minerals show the same evolution in their Eh values with the chemical composition of the starting mineralogy as the evolution documented above for pH (Table 4). The Eh values decrease from 0.347 and 0.416 V/SHE for feldspars to 0.189–0.318 V/SHE for ferromagnesian minerals. This decrease in Eh values can be ascribed to the reducing potential of ferromagnesian starting minerals that contain structural ferrous iron [Fe (II)]. Similar to pH, the Eh values of solutions in contact with Martian simulants (0.299–0.304 V/SHE; Table 4) are intermediate between those of experiments on ferromagnesian minerals and feldspars, and very close to the Eh value of experiments on clinopyroxene. As observed for pH, the mineralogical compositions of both Martian simulants do not influence the Eh values under a CO_2 atmosphere.

Regarding the experiments under ambient air, the Eh values range between 0.410 and 0.477 V/SHE (Table 4). This parameter displays the same evolution as a function of the chemical composition of the starting mineral as for the CO_2 experiments. The experiments on Martian rock simulants show Eh values of 0.450 and 0.465 V/SHE, that is, within the Eh range of experiments on individual minerals (Table 4).

3.2. The Chemical Composition of Experimental Solutions

The major elements measured in solution were Mg, Si, Ca, Na, and K, under both ambient air and CO_2 atmosphere (Figure 1 and Table S3). Aqueous Fe was measured only at low concentrations for experiments under CO_2, and aqueous Al was detected only at very low concentrations for feldspar experiments (see Figure 1 and Tables 4 and S3 for more details). In general, the aqueous concentrations of major elements appear higher in experiments under a CO_2 atmosphere than under ambient air (Figure 1). This observation is perfectly consistent with the lower pH of the solutions induced by dissolution of atmospheric CO_2. This lower pH dramatically increases the solubility of ferromagnesian minerals and, to a lesser extent, those of clinopyroxene and feldspars (Blum & Lasaga, 1991; Brady & Carroll, 1994; Chen & Brantley, 2000; Golubev et al., 2005; Pokrovsky & Schott, 2000; Schott et al., 1981; Wollast, 1967).

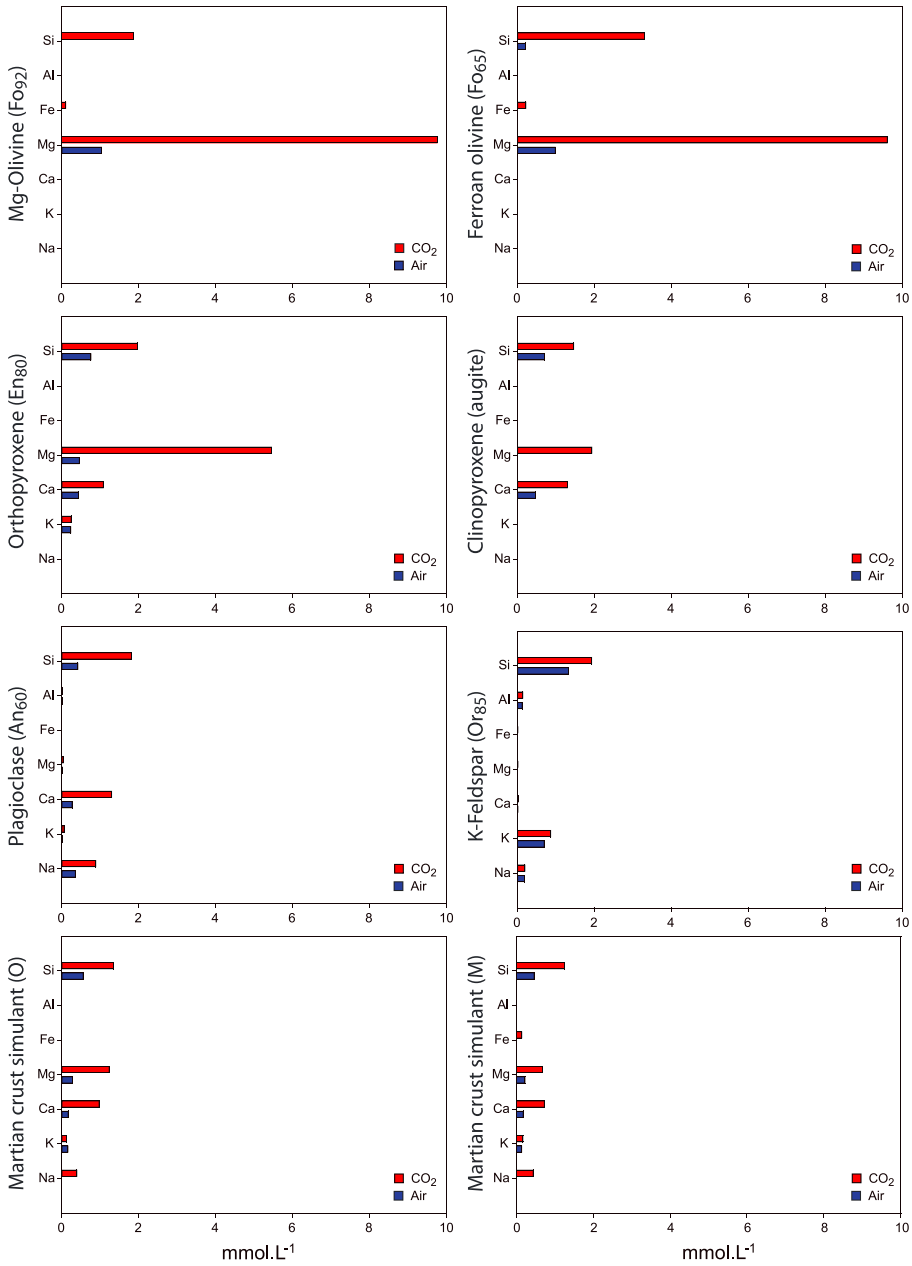

Figure 1. Concentration of major elements in experimental solutions.

The major elements measured in solution for experiments on ferromagnesian minerals are Mg, Si, and Ca (Figure 1). The aqueous concentrations of those elements are 10 to 15 times higher under a CO_2 atmosphere than under ambient air for experiments on olivines and 2 to 10 times higher for experiments on pyroxenes (Figure 1 and Table S3). For experiments on feldspars, Si, Ca, Na, and K are the major elements measured in solution, with aqueous concentrations 2 to 5 times higher under a CO_2 atmosphere than under ambient air (Figure 1 and Table S3). The experiments on the two Martian simulants show that Si, Mg, Ca, Na, and K are the major elements found in solution. The aqueous concentrations of these elements are 2 to 5 times higher under a CO_2 atmosphere than under ambient air, except for the aqueous K concentration, which is not significantly affected by the atmospheric composition (Figure 1 and Table S3).

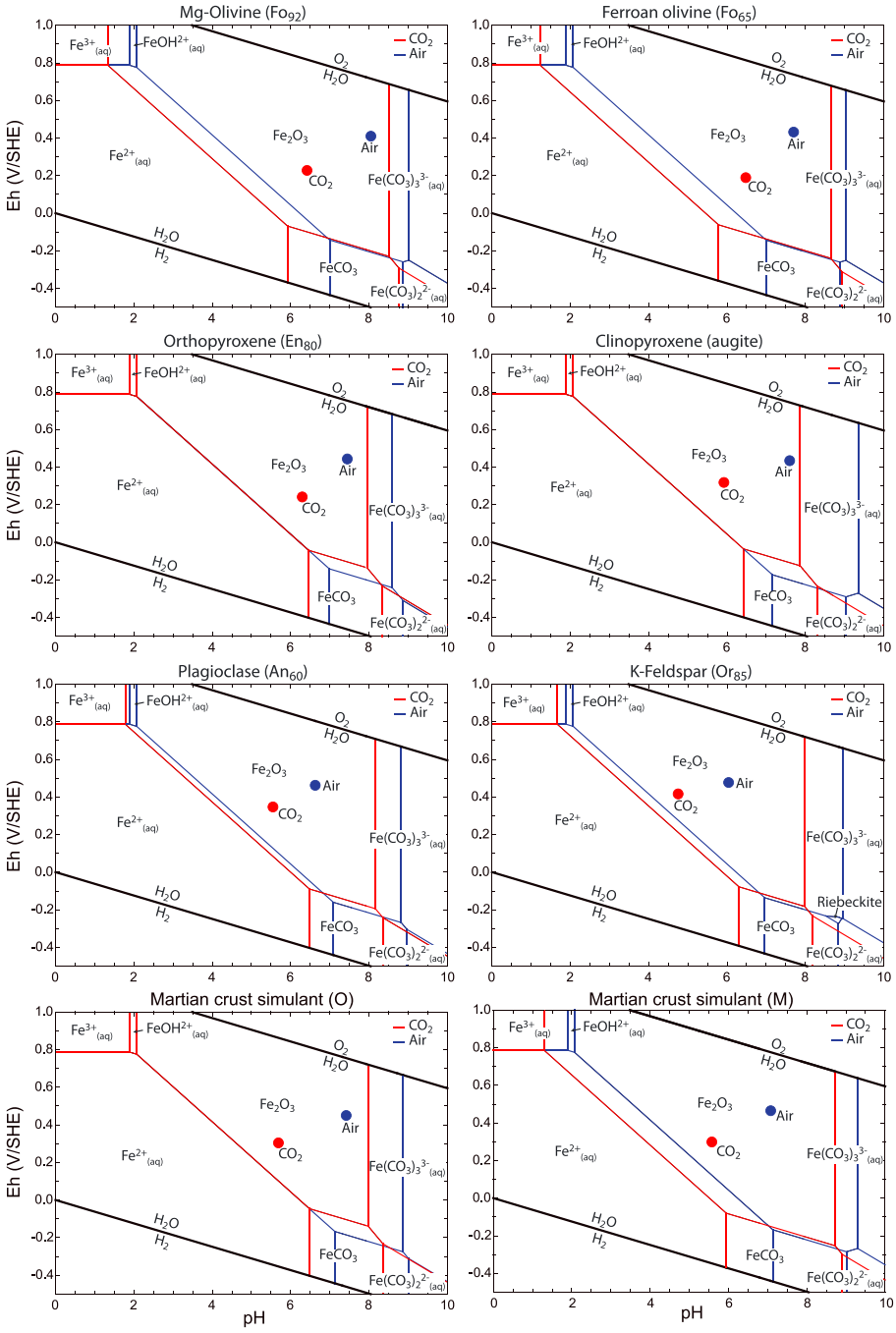

Figure 2. Eh-pH diagrams of aqueous and solid iron compounds for each experimental solution performed under ambient air and a CO_2 atmosphere at 45 °C. Each diagram is calculated using the chemical compositions of solutions presented in Table S3 in the supporting information. For solutions with no detectable aqueous Fe (i.e., for all experiments under ambient air and for experiments on clinopyroxene, orthopyroxene, plagioclase, and the Martian crust simulant (O) under a CO_2 atmosphere), the Fe concentration is fixed at 10^{-6} mol/L for calculating the diagrams.

3.3. Calculation of Eh-pH Diagrams

The Eh-pH diagrams of Figure 2 were calculated from the chemical properties and compositions of each experimental solution. The calculations were performed assuming thermodynamic equilibrium; consequently, the mineral phases predicted in equilibrium with the solution may not reflect the actual mineral products. Indeed, hematite was the thermodynamic ferric Fe [Fe (III)]-mineral in equilibrium with the

solutions; however, due to kinetic or size effects at the earlier step of weathering, other Fe (III)-compounds such as ferrihydrite or goethite could have formed in the experiments (Hochella et al., 2008; Navrotsky et al., 2008). Magnetite was not predicted in the Eh-pH diagrams due to the presence of carbonate ions favoring precipitation of Fe (II)-carbonates or the formation of ferrous carbonate aqueous species regardless of the atmospheric composition (Figure 2). Without aqueous CO_2, magnetite was predicted for high pH and very low Eh values that were not reached in our experiments.

Whether under ambient air or a CO_2 atmosphere, the Eh/pH conditions of all experiments fell inside the Fe (III)-oxide stability domain (Figure 2). These observations indicate that aqueous $Fe^{2+}_{(aq)}$ is not stable under these redox conditions of a CO_2 atmosphere and could explain the very low aqueous Fe concentration in all of the experiments. The Eh/pH diagrams and very low concentrations of aqueous Fe indicate an enrichment in this element in the solid phases and suggest potential formation of Fe (III)-bearing materials (Figures 1 and 2). Moreover, under a CO_2 atmosphere, the Eh/pH conditions of solutions are far from the stability domain of siderite ($FeCO_3$). The experiments on both Martian simulants show very similar Eh-pH conditions (Table 4 and Figure 2) despite the large difference in Fe contents and the presence of magnetite in the Martian simulant (M) (Table 1).

3.4. Estimation of the Chemical Composition of the Weathering Products

A good proxy of the weathering products can be provided by the surface layer that forms at the solid-solution interface, owing to the slow rates of dissolution and precipitation under the conditions of the present study (Figures S2 and S3). Its chemical composition can be estimated by mass balance calculations starting from the chemistry of the solution and the chemical composition of the starting mineralogy. These mass balance calculations provide a representative picture of the bulk chemistry of weathering products and an overview of the global geochemical path toward which the weathering reaction tends to proceed (Figure S4). The gain or loss of each element in the weathering products is then calculated by comparing the chemical composition of the weathering products to the stoichiometric amounts of elements dissolved from the starting materials (Figure 3). Under ambient air, these mass balance calculations indicate enrichments in Si, Fe, and Al in the weathering products, whereas alkali and alkaline earth elements (Mg, Ca, K, and Na) are depleted if starting minerals are olivines (Fo_{92} and Fo_{65}) and feldspars (plagioclase and K-feldspars; Figure 3). In contrast, the weathering products of the experiment on both pyroxenes show enrichments in Al, Fe, Mg, and Na and depletions in Si and Ca. Both Martian simulants have similar weathering trends with enrichments of the weathering products in Al, Fe, and Na, depletions in Mg, Ca, and K, and stoichiometric behavior of Si.

Under a CO_2 atmosphere, the weathering products of all experiments are Si- and Fe-enriched with respect to the starting minerals, except for the experiment on K-feldspar (Figure 3). Similar to experiments under ambient air, the weathering products in all of the experiments are enriched in Al and depleted in Mg, Ca, K, and Na, except for experiments on pyroxenes and olivines showing Na, and Ca enrichment, respectively (Figure 3).

A quite similar chemical composition is found for the weathering products formed under a dense CO_2 atmosphere and ambient air for experiments on olivines (Fo_{92} and Fo_{65}), K-feldspar, and the Martian simulant (M) (Table 5). However, those formed from pyroxenes, plagioclase, and simulant (O) indicate some differences (>5 at.%) in chemical composition depending on the atmospheric composition (Table 5). The weathering products formed on pyroxenes show the highest difference between the two atmospheres. Indeed, the weathering products formed under a CO_2 atmosphere show very high amounts of Si and very low amounts of Mg compared to those formed under ambient air (Table 5). For the experiments on plagioclase, the weathering products show an increase in Al and a decrease in Ca under a CO_2 atmosphere compared to ambient air. For Martian simulant (O), enrichments in Si and Al and depletions in Mg and Ca are observed under a CO_2 atmosphere compared to ambient air.

3.5. Thermodynamic Calculation of Saturation Index of Minerals

Thermodynamic calculations are a tool to constrain the putative mineralogy of the weathering products from the experimental solution chemistry (Table 6), bearing in mind that nucleation and crystal-growth processes at low temperature are mainly controlled by surface processes and kinetics. Moreover, thermodynamic modeling does not account for insoluble elements, which are not detected in solutions, and consequently do not reproduce the increase in some elements in the weathering products (e.g., Fe in

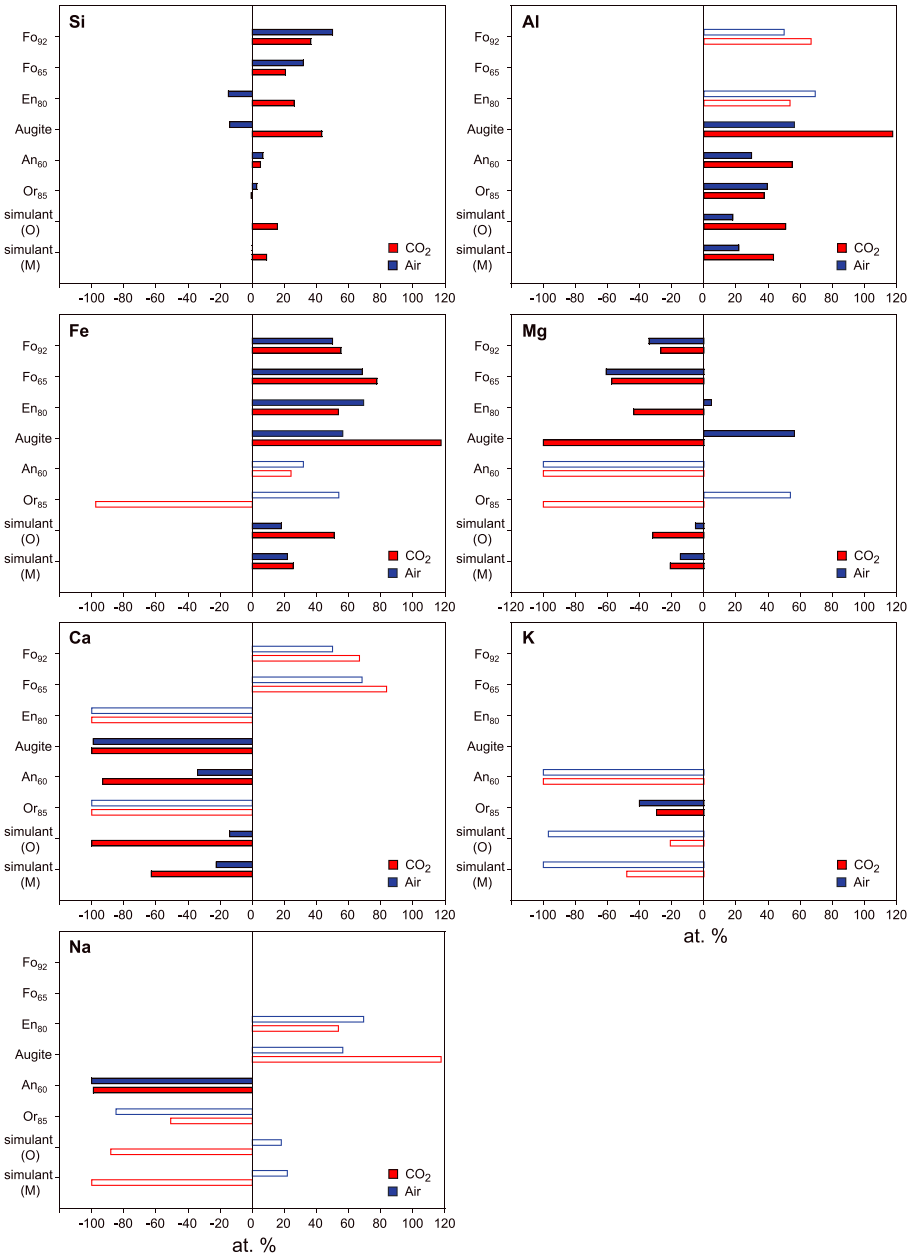

Figure 3. Percentage of atomic gain or loss of elements in the weathering products compared to the starting mineral/simulant (atomic composition). The solid bars and the open bars correspond to major elements and minor/trace elements (<5 at.%) in the chemical composition of the corresponding mineral, respectively. Mineral abbreviations: Mg-olivine (Fo_{92}); ferroan olivine (Fo_{65}); orthopyroxene (En_{80}); clinopyroxene (Augite); plagioclase (An_{60}); K-feldspar (Or_{85}); Martian crust simulant (O) (simulant (O)); Martian crust simulant (M) (simulant (M)).

experiments under ambient air or Al for a major part of the experiments). However, this modeling approach helps to discuss the presumed mineralogy that could be in contact with the experimental solutions.

3.5.1. Experiments Under Ambient Air

The experimental solutions in contact with individual minerals or simulants are in equilibrium or oversaturated with respect to common minerals described in a weathering process (Huang et al., 2011; Table 6). Indeed, the experimental solutions in contact with ferromagnesian minerals are in equilibrium or oversaturated with poorly organized Si-rich minerals, carbonates, and Mg-smectites (Table 6). The experimental solutions in contact with both feldspars (plagioclase and K-feldspar) are in equilibrium or oversaturated with poorly organized Si-rich minerals, Al-bearing minerals (zeolites, clay minerals), and Al-(oxy)hydroxides

Table 5
Difference in Estimated Chemical Composition of Weathering Products (Atomic Percentage, at. %) Between Experiments Under CO_2 and Ambient Air Atmospheres

	Ferroan olivine (Fo_{65})	Mg-olivine (Fo_{92})	Clino-pyroxene (augite)	vOrtho-pyroxene (En_{80})	Plagioclase (An_{60})	K-feldspar (Or_{85})	Martian simulant (O)	Martian simulant (M)
Si	−4.7	−3.7	27.4	20.6	−0.7	−2.1	7.5	4.1
Al	0.1	—	4.2	−0.3	7.8	−0.3	4.6	3.3
Fe	0.3	2.1	3.2	−1.0	0.0	−0.2	1.9	0.4
Mg	4.4	1.5	−36.1	−19.1	—	−0.2	−4.9	−0.8
Ca	0.0	0.0	−0.1	0.0	−7.1	−0.1	−6.9	−3.5
K	—	—	—	0.0	−0.1	1.8	1.7	1.2
Na	—	—	1.4	−0.1	0.1	1.0	−3.8	−4.7

Note. The values correspond to the atomic percentages of each element under a CO_2 atmosphere minus those under ambient air.

(Table 6). Despite the relatively low pCO_2 value under ambient air, the experimental solutions are in equilibrium or oversaturated with respect to carbonates. Note that all experimental solutions are not in equilibrium or oversaturated with Fe (III)-[(oxy)hydr]oxides or Fe (III)-bearing silicates because no Fe was detected in solutions (very low solubility of $Fe^{3+}_{(aq)}$ under oxic conditions). The experiments on simulants show the major role of olivine on the aqueous Mg concentration. This mineral produces a clear difference in the mineral saturation index between the two simulants (Table 6).

Table 6
Summary of Thermodynamic Calculations for the Saturation Indices of Minerals.

		In equilibrium	Oversaturated
Air	Mg-olivine (Fo_{92})		magnesite
	Ferroan olivine (Fo_{65})	poorly organized Si-rich minerals	magnesite, Mg-smectites (stevensite)
	Clinopyroxene (augite)	poorly organized Si-rich minerals, calcite	
	Orthopyroxene (En_{80})	poorly organized Si-rich minerals, carbonates (calcite, dolomite, magnesite)	Mg-smectites (stevensite)
	Plagioclase (An_{60})	poorly organized Si-rich minerals, zeolite	Al-smectites (beidellite, montmorillonite), zeolites, Al-rich clays minerals (kaolinite, halloysite, and imogolite), and Al-(oxy)hydroxides (gibbsite, boehmite)
	K-Feldspar (Or_{85})	poorly organized Si-rich minerals	Al-smectites (beidellite, montmorillonite), zeolites, Al-rich clays minerals (kaolinite, halloysite, and imogolite), and Al-(oxy)hydroxides (gibbsite, boehmite)
	Martian simulant (O)	poorly organized Si-rich minerals, magnesite	Mg-smectites (stevensite)
	Martian simulant (M)	poorly organized Si-rich minerals	
CO_2	Mg-olivine (Fo_{92})	poorly organized Si-rich minerals	Fe (III)-(oxyhydr)oxides (goethite, hematite, ferrihydrite, lepidocrocite, maghemite), Fe (III)-smectites (nontronite), greenrust, magnetite, carbonates (magnesite, siderite), Fe (II)/Mg-smectites (stevensite)
	Ferroan olivine (Fo_{65})	poorly organized Si-rich minerals	Fe (III)-(oxyhydr)oxides (goethite, hematite, ferrihydrite, lepidocrocite, maghemite), Fe (III)-smectites (nontronite), magnetite, greenrust, carbonates (magnesite, siderite), Fe (II)/Mg-smectites (stevensite)
	Clinopyroxene (augite)	poorly organized Si-rich minerals, magnesite	
	Orthopyroxene (En_{80})	poorly organized Si-rich minerals, carbonates (calcite, dolomite), Mg-smectites (stevensite)	Magnesite
	Plagioclase (An_{60})	poorly organized Si-rich minerals, gibbsite	Fe (III)-(oxyhydr)oxides (goethite, hematite, lepidocrocite, maghemite), Fe (III)-smectites (nontronite), Al-smectites (beidellite, montmorillonite), zeolites, Al-rich clays minerals (kaolinite, halloysite, and imogolite), and boehmite
	K-Feldspar (Or_{85})	poorly organized Si-rich minerals, gibbsite, goethite,	Fe (III)-(oxyhydr)oxides (goethite, hematite, lepidocrocite, maghemite), Fe (III)-smectites (nontronite), Al-smectites (beidellite, montmorillonite), zeolites, Al-rich clays minerals (kaolinite, halloysite, and imogolite), and boehmite
	Martian simulant (O)	poorly organized Si-rich minerals	
	Martian simulant (M)	poorly organized Si-rich minerals, greenrust, siderite	Fe (III)-[(oxi)hydr]oxides (goethite, maghemite, l epidocrocite and hematite), magnetite, Fe (III)-smectites (nontronite)

3.5.2. Experiments Under a CO_2 Atmosphere

The experimental solutions overall are in equilibrium or oversaturated with the same mineralogy as for experiments under ambient air (Table 6). The detection of Fe in several experiments (olivines, feldspars, and Martian simulant (M)) allowed the determination of the Fe-bearing minerals in equilibrium with the Eh/pH conditions of solutions. Fe (III)-bearing minerals and Fe (II, III)-oxide (magnetite) are predicted to be in equilibrium or oversaturated with respect to experimental solutions (Table 6). Fe (II)-bearing minerals (Fe (II)/Mg smectites, siderite) are also predicted to be in equilibrium with some experimental solutions (Table 6). However, these theoretical predictions are not supported by the Eh-pH diagram, where the Eh-pH conditions do not favor the formation of Fe (II)-bearing minerals (Figure 2). Indeed, in these diagrams, Fe (II, III)-oxides and Fe (II)-carbonate are out of their thermodynamic stability fields (Figure 2). In fact, the thermodynamic calculations of the mineral saturation index do not take into account the stability field of one phase with respect to another; these calculations rather indicate how far a given solution is from thermodynamic equilibrium with respect to a mineral phase.

4. Discussion

The experiments summarized in section 3 highlight five main results: (i) The experimental solutions are mildly acidic under a CO_2 atmosphere ($4.8 < pH < 6.5$), whereas the pH conditions are neutral under ambient air ($6.0 < pH < 8.1$); (ii) the redox conditions (Eh) of solutions under a CO_2 atmosphere show lower values ($0.189 < Eh < 0.416$ V/SHE) compared to solutions under ambient air ($0.410 < Eh < 0.477$ V/SHE); (iii) the Eh/pH conditions for all experiments are within the stability domain of Fe (III)-bearing minerals regardless of the atmospheric composition; (iv) the behavior of the major elements between the solid phases and the solutions deduced from mass balance calculations are similar regardless of the atmosphere except for pyroxene experiments; and (v) under a CO_2 atmosphere, alkali, and alkaline earth elements (i.e., Mg, Ca, Na, and K) and a portion of Si are leached from the starting materials into the solutions, whereas Al, Fe, and a portion of Si remain in the solid phases. Hereafter, we discuss these results and further emphasize the peculiarities of weathering under CO_2 conditions, while in section 5, we consider several implications of our study for early Mars conditions.

4.1. Geochemical Properties of Weathering Solutions Under a CO_2 Atmosphere

The differences between experiments performed under ambient air and CO_2 atmospheres provide evidence for the strong effect of the dissolution of atmospheric CO_2 on the pH of experimental solutions (Figures 1 and 2 and Table 4). Dehouck et al. (2014) and Gaudin et al. (2018) documented similar pH values (6.1 and 6.7, respectively) and a difference of approximately 2 pH units between CO_2 atmosphere and air in their weathering experiments performed under very similar conditions as ours (on the same San Carlos olivine (Fo_{92}) as in the present study).

Our experiments moreover reveal the strong effect of the starting mineralogy on the solution properties (Figures 1 and 2 and Table 4). The acidity induced by dissolution of atmospheric CO_2 is balanced by the pH buffering capacity of the starting minerals and notably by ferromagnesian silicates (Table 4). Ferromagnesian minerals are more soluble than aluminous minerals in the investigated pH range, suggesting a higher aqueous concentration of elements and a higher capacity of these minerals to buffer the acidity resulting from the CO_2 dissolution (Blum & Lasaga, 1991; Brady & Carroll, 1994; Chen & Brantley, 2000; Golubev et al., 2005; Pokrovsky & Schott, 2000; Schott et al., 1981; Wollast, 1967).

Taken as a whole, the experiments on the two simulants produce a lower total aqueous concentration of elements than the experiments on individual minerals (Figure 1), despite the high proportion of ferromagnesian minerals present in these simulants and the lower pH. A lower total aqueous concentration of elements can reflect the competition between dissolution rates of each starting mineral and precipitation rates of secondary minerals in a complex mineral assemblage composed by mixing individual mineral particles (Oelkers & Schott, 2009).

The chemical compositions of experimental solutions under a CO_2 atmosphere indicate a leaching of alkali and alkaline earth elements as well as of Si, whereas the concentrations of aqueous Al and Fe are near zero. Nevertheless, the comparison of the alkali and alkaline earth elements over the Si ratio between the starting materials and solutions indicates the Si-enrichment in the weathering products. This chemical weathering

trend under a CO_2 atmosphere is in good agreement with the results obtained by Fabre et al. (2011) on the experimental weathering of basalts under a Precambrian atmosphere (i.e., 90% N_2 and 10% CO_2).

For experiments in which Fe was detected in solutions under a CO_2 atmosphere, the Eh/pH diagrams indicate that the Eh/pH conditions of solutions fall within the stability domain of Fe (III)-bearing minerals. The data show that ferromagnesian minerals have clear redox buffering compared to feldspars (Table 4). It can be deduced from these results that redox conditions (Eh) are partly controlled by the Fe^{2+}/Fe^{3+} redox couple. From these equilibrium thermodynamic calculations, the Eh/pH data show that $Fe^{2+}_{(aq)}$ or Fe (II) (from the solutions or the solid phases, respectively) are oxidized under a CO_2 atmosphere to potentially form Fe (III)-bearing minerals. However, Fe (II)-bearing minerals cannot be completely ruled out because the Fe (II)-mineral formation rate competes with the hydrolysis rate of primary minerals and the Fe (III) oxidation rate (Neubeck et al., 2014). Nonetheless, the thermodynamic equilibrium tends to support the oxidation of Fe (II), as shown by the thermodynamic calculations of the Eh/pH diagrams and the saturation indices of minerals (Figure 2 and Table 6).

Chevrier et al. (2004, 2006), Dehouck et al. (2012), and Gaudin et al. (2018) documented a similar trend of Fe oxidation during weathering experiments on ferrous minerals at low temperatures. Indeed, these authors observed the formation of Fe (III)-bearing minerals (e.g., goethite, ferrihydrite, Fe (III)-smectites) as weathering products of Fe (II)-sulfur or Fe (II)-silicates (e.g., pyrrhotite, olivine, and pyroxenes) under a CO_2- and water-rich atmosphere.

4.2. Chemical Composition of Weathering Products Under a CO_2 Atmosphere

Taken as a whole, the chemical compositions of the weathering products are similar for experiments under ambient air and a CO_2 atmosphere on the same starting material, except for the experiments on pyroxenes (Figure S1). The variability of the geochemical trends of elements between weathering products and the solution can be explained by several parameters, such as the pH-Eh conditions, the composition and structure of starting minerals, the kinetics of dissolution of the starting material, and the kinetics of precipitation of the weathering products (Oelkers & Schott, 2009). Under a CO_2 atmosphere, the weathering products are enriched in Si, Al, and Fe compared to the chemical composition of the starting minerals or the simulants (Figure 3). This observation is in good agreement with the weathering products identified in previous studies on basaltic rocks or ferromagnesian and feldspars minerals under low temperature and a CO_2-rich atmosphere (<1 atm CO_2; Busenberg, 1978; Fabre et al., 2011; Gaudin et al., 2018).

The thermodynamic calculations predict equilibrium or oversaturation with respect to a similar mineralogy for the experiments on individual minerals and the simulant (M) between ambient air and a CO_2 atmosphere (Table 6), although the pH conditions are different. These results of thermodynamic calculations are consistent with the estimated chemistry of weathering products that does not display large variations between the two atmospheres. Accordingly, the thermodynamic model and the Eh/pH diagrams predict the possibility for Fe (III)-bearing minerals to form, notably as Fe (III)-smectites. Our results agree well with the general weathering trend (Figure 4) and the results obtained by Gaudin et al. (2018).

For the simulant (O), the major difference between the two atmospheres is the equilibrium or oversaturation of the solution with magnesite and Mg-rich smectites under ambient air. This result can be explained by the lower pH values of the solutions in contact with atmospheric CO_2 (5.75 vs. 7.47 under ambient air) that significantly increase the solubility of Mg-smectites and carbonates and thus reduce their formation rates at this low pH value (Murakami et al., 2004; Tosca et al., 2008). This result strongly supports those of Dehouck et al. (2014) and Gaudin et al. (2018), who documented a dramatic decrease in the formation of smectites under a CO_2 atmosphere, balanced by increasing amounts of amorphous silica phases.

5. Implications for Early Martian Surface Conditions

5.1. Constraints on Geochemical Properties of Weathering Solutions

Our experiments on Martian simulants under a dense CO_2 atmosphere can provide additional constraints on the Eh/pH conditions for early Martian weathering. The weakly acidic pH of the solutions (5.6) could be considered as the highest pH value for surface water in contact with a dense CO_2 atmosphere and an early Martian crust mineral composition. Indeed, our experiments did not involve SO_2, H_2S, or HCl, which

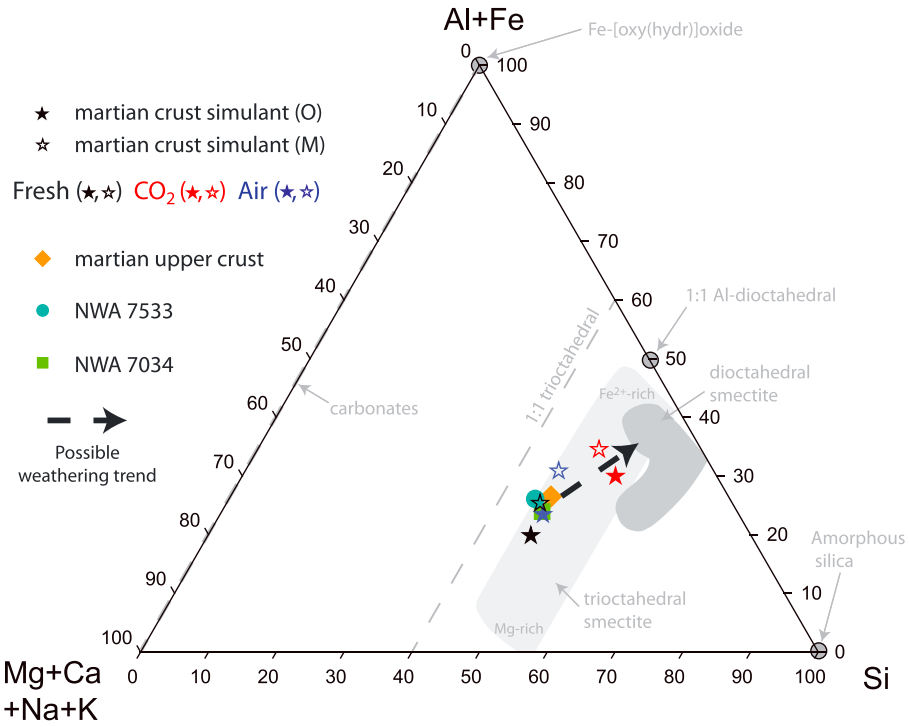

Figure 4. Ternary diagrams Si-Al/Fe-Mg/Ca/Na/K showing the composition (at.%) of the starting Martian crust simulants and the calculated compositions of the weathering products for the experiments under ambient air and a CO_2 atmosphere. The chemical composition of the Mars upper crust and the impact regolith breccia meteorites NWA 7533 and NWA 7034 come from Taylor and McLennan (2009), Humayun et al. (2013), and Agee et al. (2013), respectively.

were most likely present, at least episodically, as volcanic gases in early Mars atmosphere (Sholes et al., 2017) and could have significantly decreased the pH of the solutions. The redox conditions of our experiments coupled with Eh/pH diagrams indicate that Fe should oxidize regardless of the Fe content of the starting Martian simulant. Numerous studies under anoxic environments or very low oxygen fugacity have reported the oxidation of Fe through Schikorr's reaction ($Fe^{2+}_{(aq)} + H_3O^+_{(aq)} \rightarrow Fe^{3+}_{(aq)} + 1/2H_{2(g)} + H_2O_{(aq)}$), whether in low-temperature (25 to 100 °C) water-rock interactions in the laboratory (e.g., Mayhew et al., 2013; McCollom & Donaldson, 2016) or in the field (Proskurowski et al., 2008). These geochemical properties of solutions, including acidity and redox conditions, could reveal some possible trends in the solution properties of the surface waters in contact with Martian basaltic rocks on the surface of early Mars.

The experiments on the two simulants under a CO_2 atmosphere allow us to constrain the aqueous geochemistry of the Martian surface water in contact with the primordial Martian atmosphere and the putative primordial Martian crust as recomputed by Humayun et al. (2013), Sautter et al. (2015), and Taylor and McLennan (2009). These interactions could produce percolating waters enriched in dissolved inorganic carbon, silica, and alkali and alkaline earth elements. The dominant aqueous species would be $H_2CO_{3\ (aq)} > HCO_3^-{}_{(aq)} > H_4SiO_{4(aq)} > Mg^{2+}_{(aq)} > Ca^{2+}_{(aq)} > Na^+_{(aq)} > K^+_{(aq)}$ for the simulant (O); for the simulant (M), the dominant species in solution would be $H_2CO_{3\ (aq)} > HCO_3^-{}_{(aq)} > H_4SiO_{4(aq)} > Ca^{2+}_{(aq)} > Mg^{2+}_{(aq)} > Na^+_{(aq)} > K^+_{(aq)} > Fe^{2+}_{(aq)}$.

5.2. Constraints on the Intensity of Chemical Weathering

Chemical weathering is an intricate process that destabilizes primary minerals through a combination of mechanisms such as dissolution, carbonation, hydrolysis, and redox processes. In this process, the major weathering agents are water and atmospheric gases that involve leaching into solution a part of elements from the original mineral, whereas the other part remains in the weathering products.

Assuming that alkalinity (considered here as the activity of HCO_3^- and CO_3^{2-} aqueous species) is a good indicator of the chemical weathering intensity, that is, the capacity of a solution to attack a mineral or a rock, the alkalinity of solutions appears clearly higher under an early Martian atmosphere than under ambient air. Indeed, the solutions of experiments on individual minerals have alkalinities 2 to 10 times higher under CO_2 than under ambient air depending on the nature of the mineral (9.2–9.5 for olivines, 6.4–6.8 for pyroxenes, and 1.6–3.9 for feldspars). The solutions from the experiments on Martian simulants have alkalinities 4 to 4.5 times higher under the likely primordial compositions of the Martian atmosphere than under present Earth atmosphere, given the conditions of the present study. These values of chemical weathering intensity are in agreement with those obtained by Fabre et al. (2011) on flood basalts under an anoxic atmosphere (90% N_2 and 10% CO_2) despite the lower concentration of atmospheric CO_2 than in our experiments.

5.3. Constraints on the Chemistry and Mineralogy of Weathering Products

The weathering trend can be depicted by a ternary plot of the chemical compositions of the weathering products compared to the bulk composition of the unweathered Martian crust simulants and the different estimates of the Martian upper crust (Taylor & McLennan, 2009; Agee et al., 2013; Hewins et al., 2017; Figure 4). Despite the great differences in Fe content between the two Martian simulants, the weathering trends and the chemical weathering intensities appear similar and of the same order of magnitude (Figure 4). Even produced in closed system experiments, the enrichment of weathering products in insoluble elements (Al, Fe, and to a lesser extent Si) compared to the unweathered initial simulants reproduces quite well the geochemical trend observed in some weathering profiles on Earth (i.e., depletions in Si and alkali and alkaline earth elements and enrichments in Al and Fe; Gaudin et al., 2011 and references therein). On Mars, some sequences of Al-rich clay minerals overlapping Fe/Mg clay minerals have been observed in many locations from orbital detections and interpreted in terms of weathering profiles (e.g., Bishop et al., 2018; Carter et al., 2015; Gaudin et al., 2011; Loizeau et al., 2007, 2010, 2018). The similarities in the chemical weathering trends obtained in our experiments, whether under terrestrial ambient air or a CO_2 atmosphere, suggest that such putative weathering profiles could have developed very early on Mars. Likewise, recent in situ analyses made by the *Curiosity* rover indicate altered sediments in an open system, perhaps before their emplacement in Gale crater (Bristow et al., 2018; Mangold et al., 2019).

Fe-bearing clay minerals have also been widely identified at the surface of Mars from orbital data (Carter et al., 2015). Many of these detections were interpreted as Fe (III)-smectites, such as nontronite, resulting from water/rock interactions under surface or subsurface conditions (Ehlmann et al., 2011; Michalski et al., 2015; Milliken & Bish, 2010; Murchie et al., 2009; Mustard et al., 2008; Poulet et al., 2008; Roach et al., 2010). Our thermodynamic calculations on experimental solutions provide experimental support for these observations in predicting the possible formation of Fe (III)-bearing minerals, notably Fe (III)-smectites, which agree with the Eh/pH diagrams and the results obtained by Gaudin et al. (2018). As shown by our experiments, the chemistry of weathering products actually tends toward a theoretical chemical composition of Al-Fe (III)-rich clay minerals (Figure 4). Fe (III)-smectites have potentially formed from low-temperature water/rock interactions under anoxic conditions, that is, the inferred conditions for surface solutions on early Mars.

5.4. Constraints on Carbonates Under a Dense CO_2 Atmosphere

The results of the present study place further constraints on the hotly debated issue of whether carbonates precipitated or not in the early Mars surface environment. Of course, the paucity of carbonates detected with remote-sensing methods from orbit (Wray et al., 2016, and references therein) cannot be reconciled with previous thermodynamic modeling of silicate weathering that predicted the formation of carbonates (e.g., Zolotov & Mironenko, 2016). The occurrence of Martian surface carbonates remains controversial. Carbonates have been identified in soils at the Phoenix landing site and interpreted as resulting from the interaction of atmospheric CO_2 with liquid water films on soil particles (Boynton et al., 2009). In contrast, most orbital carbonate detections, such as in the Nili Fossae region and carbonate-rich outcrops in the Gusev crater, have been interpreted as the result of hydrothermal activity in olivine-rich bedrock (Brown et al., 2010; Morris et al., 2010; Niles et al., 2013; Turner et al., 2016). The *Curiosity* rover has not documented high proportions of carbonates in Gale crater rocks (<1 wt.%, Sutter et al., 2017), despite the presence of alteration minerals (locally up to 25 wt.% of phyllosilicates) in aqueously altered fine-grained sedimentary rocks (Bristow et al., 2018; Rampe et al., 2017).

Dehouck et al. (2014) detected only a very small amount of carbonate in their experiments despite the high pH buffering and the high Mg concentration of the starting mineral (San Carlos olivine, Fo_{92}). For experiments on the same starting olivine, however, Gaudin et al. (2018) identified the formation of approximately 3 wt.% of carbonates, but the pH of their experimental solutions was clearly higher (6.8 compared to 6 for Dehouck et al., 2014). This discrepancy can be ascribed to the lower pH value of the solutions that enhance the solubility of carbonates. Our experiments document strong leaching (alkali and alkaline earth elements) and some potential oxidation (Fe (II)) of elements that enter into the composition of carbonates. Taken as a whole, both compositional and intensive parameters such as redox and pH inhibit or dramatically reduce carbonate formation even under conditions of a dense CO_2 early Mars atmosphere and despite suitable experimental conditions (i.e., closed system, high pCO_2, and no competition with other anions). Considering a weathering process developed on basaltic Martian rocks under a dense CO_2 atmosphere, the formation of carbonates appears unlikely when atmospheric control dominates the chemical properties of the percolating solutions. However, once this control is over (i.e., porous solutions not connected to the atmosphere), the high buffering of the Martian rock-forming minerals on pH and Eh could favor the formation of carbonates.

6. Conclusions

Low-temperature experimental weathering on Martian crust simulants was performed under an anoxic CO_2 atmosphere to constrain the potential weathering conditions that could have occurred during early Mars period. For this purpose, two simulants were prepared from selected Martian mineral analogs, taking into account recent results on Martian regolith breccia meteorites and in situ observations in Gale crater.

The experimental weathering solutions in contact with the martian crust simulants bear evidence for a large effect of the dense CO_2 atmosphere, notably on the pH. Indeed, acidic conditions are evidenced for both experiments on martian crust simulants. These acidic conditions are reached only though the effect of atmospheric CO_2 dissolution without any other acidic agents, such as sulfuric acid or hydrochloric acid.

The acidic conditions occurring during weathering experiments yield strong leaching of alkali and alkaline elements (Mg, Ca, Na, and K). Silicon and Fe are also found in the solution. However, the mass balance calculations indicate an enrichment of the solid materials in Al, Fe, and Si compared to the bulk initial composition. This weathering trend is similar to those currently observed on Earth, but the intensity of the chemical weathering under a dense CO_2 atmosphere appears to be 4 times higher than that under ambient air, given the conditions of the present study. In addition, the redox state of the solutions coupled with thermodynamic calculations indicate that experimental solutions are in equilibrium or oversaturated with Fe (III)-bearing minerals. This results means that at equilibrium, Fe (II) should oxidize despite the anoxic conditions that prevail in our experiments.

The combination of the acidic conditions, the strong leaching of alkali and alkaline earth elements, and the potential Fe oxidation clearly shows that weathering conditions with respect to Martian crust simulants are not suitable for carbonate formation despite a dense CO_2 atmosphere. The experimental weathering on the Martian crust simulant provides some important constraints on the possible weathering conditions that could have occurred on early Mars. The geochemical trend determined from the present experimental weathering could support the orbital Martian observations that suggest potential weathering profiles with geochemical trends similar to those observed on Earth (e.g., Carter et al., 2015; Gaudin et al., 2011).

Acknowledgments
Comments from two anonymous reviewers and a JGR Associate Editor considerably improved the manuscript. We acknowledge the support from the Agence Nationale de la Recherche (ANR) under the contract ANR-16-CE31-0012 entitled Mars-Prime. We acknowledge C. Ballhaus and B. Rondeau for providing some of the starting minerals. We thank Laurent Lenta for the preparation of the polished section of starting minerals, Marion Rivoal for her help during ICP-AES analyses, Erwan Le Menn for his help during the development of the experimental setup, Nicolas Stephant and Sylvain Pont for their help during SEM analyses, and Pierre-Emmanuel Petit for his help during XRD analyses. All data used in this manuscript are available in the Supporting information.

References

Achille, G. D., & Hynek, B. M. (2010). Ancient ocean on Mars supported by global distribution of deltas and valleys. *Nature Geoscience*, *3*(7), 459–463. https://doi.org/10.1038/ngeo891

Agee, C. B., Wilson, N. V., McCubbin, F. M., Ziegler, K., Polyak, V. J., Sharp, Z. D., et al. (2013). Unique meteorite from early Amazonian Mars: Water-rich basaltic breccia Northwest Africa 7034. *Science*, *339*(6121), 780–785. https://doi.org/10.1126/science.1228858

Ansan, V., Loizeau, D., Mangold, N., le Mouélic, S., Carter, J., Poulet, F., et al. (2011). Stratigraphy, mineralogy, and origin of layered deposits inside Terby crater, Mars. *Icarus*, *211*(1), 273–304. https://doi.org/10.1016/j.icarus.2010.09.011

Bandfield, J. L. (2002). Global mineral distributions on Mars. *Journal of Geophysical Research*, *107*(E6), 5042. https://doi.org/10.1029/2001JE001510

Banfield, J. F., & Eggleton, R. A. (1990). Analytical transmission electron microscope studies of plagioclase, muscovite, and K-feldspar weathering. *Clays and Clay Minerals*, *38*(1), 77–89. https://doi.org/10.1346/CCMN.1990.0380111

Bibring, J.-P., Langevin, Y., Gendrin, A., Gondet, B., Poulet, F., Berthé, M., et al., & OMEGA team (2005). Mars surface diversity as revealed by the OMEGA/Mars Express observations. *Science*, *307*(5715), 1576–1581. https://doi.org/10.1126/science.1108806

Bibring, J.-P., Langevin, Y., Mustard, J. F., Poulet, F., Arvidson, R., Gendrin, A., et al. (2006). Global mineralogical and aqueous Mars history derived from OMEGA/Mars Express data. *Science*, *312*(5772), 400–404. https://doi.org/10.1126/science.1122659

Bishop, J. L., Fairén, A. G., Michalski, J. R., Gago-Duport, L., Baker, L. L., Velbel, M. A., et al. (2018). Surface clay formation during short-term warmer and wetter conditions on a largely cold ancient Mars. *Nature Astronomy*, *2*(3), 206–213. https://doi.org/10.1038/s41550-017-0377-9

Blanc, P., Vieillard, P., Gailhanou, H., Gaboreau, S., Gaucher, É., Fialips, C. I., et al. (2015). A generalized model for predicting the thermodynamic properties of clay minerals. *American Journal of Science*, *315*(8), 734–780. https://doi.org/10.2475/08.2015.02

Blum, A. E., & Lasaga, A. C. (1991). The role of surface speciation in the dissolution of albite. *Geochimica et Cosmochimica Acta*, *55*(8), 2193–2201. https://doi.org/10.1016/0016-7037(91)90096-N

Boynton, W. V., Ming, D. W., Kounaves, S. P., Young, S. M. M., Arvidson, R. E., Hecht, M. H., et al. (2009). Evidence for calcium carbonate at the Mars phoenix landing site. *Science*, *325*(5936), 61–64. https://doi.org/10.1126/science.1172768

Brady, P. V., & Carroll, S. A. (1994). Direct effects of CO2 and temperature on silicate weathering: Possible implications for climate control. *Geochimica et Cosmochimica Acta*, *58*(7), 1853–1856. https://doi.org/10.1016/0016-7037(94)90543-6

Bristow, T. F., Rampe, E. B., Achilles, C. N., Blake, D. F., Chipera, S. J., Craig, P., et al. (2018). Clay mineral diversity and abundance in sedimentary rocks of Gale crater, Mars. *Science Advances*, *4*(6), eaar3330. https://doi.org/10.1126/sciadv.aar3330

Brown, A. J., Hook, S. J., Baldridge, A. M., Crowley, J. K., Bridges, N. T., Thomson, B. J., et al. (2010). Hydrothermal formation of Clay-Carbonate alteration assemblages in the Nili Fossae region of Mars. *Earth and Planetary Science Letters*, *297*(1-2), 174–182. https://doi.org/10.1016/j.epsl.2010.06.018

Busenberg, E. (1978). The products of the interaction of feldspars with aqueous solutions at 25°C. *Geochimica et Cosmochimica Acta*, *42*(11), 1679–1686. https://doi.org/10.1016/0016-7037(78)90256-9

Carter, J., Poulet, F., Bibring, J.-P., Mangold, N., & Murchie, S. (2013). Hydrous minerals on Mars as seen by the CRISM and OMEGA imaging spectrometers: Updated global view. *Journal of Geophysical Research: Planets*, *118*, 831–858. https://doi.org/10.1029/2012JE004145

Carter, J., Loizeau, D., Mangold, N., Poulet, F., & Bibring, J.-P. (2015). Widespread surface weathering on early Mars: A case for a warmer and wetter climate. *Icarus*, *248*, 373–382. https://doi.org/10.1016/j.icarus.2014.11.011

Chen, Y., & Brantley, S. L. (2000). Dissolution of forsteritic olivine at 65°C and 2. *Chemical Geology*, *165*(3), 267–281. https://doi.org/10.1016/S0009-2541(99)00177-1

Chevrier, V., Mathé, P.-E., Rochette, P., Grauby, O., Bourrié, G., & Trolard, F. (2006). Iron weathering products in a CO_2+(H_2O or H_2O_2) atmosphere: Implications for weathering processes on the surface of Mars. *Geochimica et Cosmochimica Acta*, *70*(16), 4295–4317. https://doi.org/10.1016/j.gca.2006.06.1368

Chevrier, V., Rochette, P., Mathé, P.-E., & Grauby, O. (2004). Weathering of iron-rich phases in simulated Martian atmospheres. *Geology*, *32*(12), 1033–1036. https://doi.org/10.1130/G21078.1

Craddock, R. A., & Howard, A. D. (2002). The case for rainfall on a warm, wet early Mars. *Journal of Geophysical Research*, *107*(E11), 5111. https://doi.org/10.1029/2001JE001505

Craddock, R. A., Maxwell, T. A., & Howard, A. D. (1997). Crater morphometry and modification in the Sinus Sabaeus and Margaritifer Sinus regions of Mars. *Journal of Geophysical Research*, *102*(E6), 13321–13340. https://doi.org/10.1029/97JE01084

Daval, D., Sissmann, O., Menguy, N., Saldi, G. D., Guyot, F., Martinez, I., et al. (2011). Influence of amorphous silica layer formation on the dissolution rate of olivine at 90°C and elevated pCO_2. *Chemical Geology*, *284*(1-2), 193–209. https://doi.org/10.1016/j.chemgeo.2011.02.021

Dehouck, E., Chevrier, V., Gaudin, A., Mangold, N., Mathé, P.-E., & Rochette, P. (2012). Evaluating the role of sulfide-weathering in the formation of sulfates or carbonates on Mars. *Geochimica et Cosmochimica Acta*, *90*, 47–63. https://doi.org/10.1016/j.gca.2012.04.057

Dehouck, E., Gaudin, A., Chevrier, V., & Mangold, N. (2016). Mineralogical record of the redox conditions on early Mars. *Icarus*, *271*, 67–75. https://doi.org/10.1016/j.icarus.2016.01.030

Dehouck, E., Gaudin, A., Mangold, N., Lajaunie, L., Dauzères, A., Grauby, O., & Le Menn, E. (2014). Weathering of olivine under CO_2 atmosphere: A Martian perspective. *Geochimica et Cosmochimica Acta*, *135*, 170–189. https://doi.org/10.1016/j.gca.2014.03.032

Ehlmann, B. L., Berger, G., Mangold, N., Michalski, J. R., Catling, D. C., Ruff, S. W., et al. (2013). Geochemical consequences of widespread clay mineral formation in Mars' ancient crust. *Space Science Reviews*, *174*(1-4), 329–364. https://doi.org/10.1007/s11214-012-9930-0

Ehlmann, B. L., Mustard, J. F., Murchie, S. L., Bibring, J.-P., Meunier, A., Fraeman, A. A., & Langevin, Y. (2011). Subsurface water and clay mineral formation during the early history of Mars. *Nature*, *479*(7371), 53–60. https://doi.org/10.1038/nature10582

Fabre, S., Berger, G., & Nédélec, A. (2011). Modeling of continental weathering under high-CO_2 atmospheres during Precambrian times. *Geochemistry, Geophysics, Geosystems*, *12*, Q10001. https://doi.org/10.1029/2010GC003444

Gaudin, A., Dehouck, E., Grauby, O., & Mangold, N. (2018). Formation of clay minerals on Mars: Insights from long-term experimental weathering of olivine. *Icarus*, *311*, 210–223. https://doi.org/10.1016/j.icarus.2018.01.029

Gaudin, A., Dehouck, E., & Mangold, N. (2011). Evidence for weathering on early Mars from a comparison with terrestrial weathering profiles. *Icarus*, *216*(1), 257–268. https://doi.org/10.1016/j.icarus.2011.09.004

Golubev, S. V., Pokrovsky, O. S., & Schott, J. (2005). Experimental determination of the effect of dissolved CO_2 on the dissolution kinetics of Mg and Ca silicates at 25 °C. *Chemical Geology*, *217*(3-4), 227–238. https://doi.org/10.1016/j.chemgeo.2004.12.011

Grotzinger, J. P., Gupta, S., Malin, M. C., Rubin, D. M., Schieber, J., Siebach, K., et al. (2015). Deposition, exhumation, and paleoclimate of an ancient lake deposit, Gale crater, Mars. *Science*, *350*(6257), aac7575. https://doi.org/10.1126/science.aac7575

Grotzinger, J. P., Sumner, D. Y., Kah, L. C., Stack, K., Gupta, S., Edgar, L., et al. (2014). A habitable fluvio-lacustrine environment at Yellowknife Bay, Gale crater, Mars. *Science*, *343*(6169), 1242777. https://doi.org/10.1126/science.1242777

Hewins, R. H., Zanda, B., Humayun, M., Lorand, J.-P., Deldicque, D., Pont, S., et al. (2013). *Petrology of NWA 7533: Formation by impacts on ancient Martian crust.Meteoritics & Planetary Science*, *48*(s1), 5252. https://doi.org/10.1111/maps.12165

Hewins, R. H., Zanda, B., Humayun, M., Nemchin, A., Lorand, J.-P., Pont, S., et al. (2017). Regolith breccia Northwest Africa 7533: Mineralogy and petrology with implications for early Mars. *Meteoritics & Planetary Science*, *52*(1), 89–124. https://doi.org/10.1111/maps.12740

Hochella, M. F., Lower, S. K., Maurice, P. A., Penn, R. L., Sahai, N., Sparks, D. L., & Twining, B. S. (2008). Nanominerals, mineral nanoparticles, and earth systems. *Science*, *319*(5870), 1631–1635. https://doi.org/10.1126/science.1141134

Huang, P. M., Li, Y., & Sumner, M. E. (Eds) (2011). *Handbook of soil sciences: Properties and processes*. CRC Press.

Humayun, M., Nemchin, A., Zanda, B., Hewins, R. H., Grange, M., Kennedy, A., et al. (2013). Origin and age of the earliest Martian crust from meteorite NWA 7533. *Nature*, *503*(7477), 513–516. https://doi.org/10.1038/nature12764

Jakosky, B. M., Brain, D., Chaffin, M., Curry, S., Deighan, J., Grebowsky, J., et al. (2018). Loss of the Martian atmosphere to space: Present-day loss rates determined from MAVEN observations and integrated loss through time. *Icarus*, *315*, 146–157. https://doi.org/10.1016/j.icarus.2018.05.030

van der Lee, J. (1998). Thermodynamic and mathematical concepts of CHESS.

Le Bas, M. J., Le Maitre, R. W., Streckeisen, A., & Zanettin, B. (1986). A Chemical Classification of Volcanic Rocks Based on the TotalAlkali-Silica Diagram. *Journal ofPetrology*, *27*(3), 745–750. https://doi.org/10.1093/petrology/27.3.745

Loizeau, D., Mangold, N., Poulet, F., Ansan, V., Hauber, E., Bibring, J.-P., et al. (2010). Stratigraphy in the Mawrth Vallis region through OMEGA, HRSC color imagery and DTM. *Icarus*, *205*(2), 396–418. https://doi.org/10.1016/j.icarus.2009.04.018

Loizeau, D., Mangold, N., Poulet, F., Bibring, J.-P., Gendrin, A., Ansan, V., et al. (2007). Phyllosilicates in the Mawrth Vallis region of Mars. *Journal of Geophysical Research*, *112*, E08S08. https://doi.org/10.1029/2006JE002877

Loizeau, D., Quantin-Nataf, C., Carter, J., Flahaut, J., Thollot, P., Lozac'h, L., & Millot, C. (2018). Quantifying widespread aqueous surface weathering on Mars: The plateaus south of Coprates Chasma. *Icarus*, *302*, 451–469. https://doi.org/10.1016/j.icarus.2017.11.002

Mangold, N., Adeli, S., Conway, S., Ansan, V., & Langlais, B. (2012). A chronology of early Mars climatic evolution from impact crater degradation. *Journal of Geophysical Research*, *117*, E04003. https://doi.org/10.1029/2011JE004005

Mangold, N., Dehouck, E., Fedo, C., Forni, O., Achilles, C., Bristow, T., et al. (2019). Chemical alteration of fine-grained sedimentary rocks at Gale crater. *Icarus*, *321*, 619–631. https://doi.org/10.1016/j.icarus.2018.11.004

Mangold, N., Thompson, L. M., Forni, O., Williams, A. J., Fabre, C., le Deit, L., et al. (2016). Composition of conglomerates analyzed by the Curiosity rover: Implications for Gale crater crust and sediment sources. *Journal of Geophysical Research: Planets*, *121*, 353–387. https://doi.org/10.1002/2015JE004977

Marcucci, E. C., & Hynek, B. M. (2014). Laboratory simulations of acid-sulfate weathering under volcanic hydrothermal conditions: Implications for early Mars. *Journal of Geophysical Research: Planets*, *119*, 679–703. https://doi.org/10.1002/2013JE004439

Mayhew, L. E., Ellison, E. T., McCollom, T. M., Trainor, T. P., & Templeton, A. S. (2013). Hydrogen generation from low-temperature water–rock reactions. *Nature Geoscience*, *6*(6), 478–484. https://doi.org/10.1038/ngeo1825

McCollom, T. M., & Donaldson, C. (2016). Generation of Hydrogen and Methane during experimental low-temperature reaction of ultramafic rocks with water. *Astrobiology*, *16*(6), 389–406. https://doi.org/10.1089/ast.2015.1382

McCubbin, F. M., Boyce, J. W., Novák-Szabó, T., Santos, A. R., Tartèse, R., Muttik, N., et al. (2016). Geologic history of Martian regolith breccia Northwest Africa 7034: Evidence for hydrothermal activity and lithologic diversity in the Martian crust. *Journal of Geophysical Research: Planets*, *121*, 2120–2149. https://doi.org/10.1002/2016JE005143

Michalski, J. R., Cuadros, J., Bishop, J. L., Darby Dyar, M., Dekov, V., & Fiore, S. (2015). Constraints on the crystal-chemistry of Fe/Mg-rich smectitic clays on Mars and links to global alteration trends. *Earth and Planetary Science Letters*, *427*, 215–225. https://doi.org/10.1016/j.epsl.2015.06.020

Milliken, R. E., & Bish, D. L. (2010). Sources and sinks of clay minerals on Mars. *Philosophical Magazine*, *90*(17–18), 2293–2308. https://doi.org/10.1080/14786430903575132

Morris, R. V., Ruff, S. W., Gellert, R., Ming, D. W., Arvidson, R. E., Clark, B. C., et al. (2010). Identification of carbonate-rich outcrops on Mars by the Spirit Rover. *Science*, *329*(5990), 421–424. https://doi.org/10.1126/science.1189667

Morrison, S. M., Downs, R. T., Blake, D. F., Vaniman, D. T., Ming, D. W., Hazen, R. M., et al. (2018). Crystal chemistry of Martian minerals from Bradbury Landing through Naukluft Plateau, Gale crater, Mars. *American Mineralogist*, *103*(6), 857–871. https://doi.org/10.2138/am-2018-6124

Murakami, T., Ito, J.-I., Utsunomiya, S., Kasama, T., Kozai, N., & Ohnuki, T. (2004). Anoxic dissolution processes of biotite: Implications for Fe behavior during Archean weathering. *Earth and Planetary Science Letters*, *224*(1-2), 117–129. https://doi.org/10.1016/j.epsl.2004.04.040

Murchie, S. L., Mustard, J. F., Ehlmann, B. L., Milliken, R. E., Bishop, J. L., McKeown, N. K., et al. (2009). A synthesis of Martian aqueous mineralogy after 1 Mars year of observations from the Mars Reconnaissance Orbiter. *Journal of Geophysical Research*, *114*, E00D06. https://doi.org/10.1029/2009JE003342

Mustard, J. F., Poulet, F., Gendrin, A., Bibring, J.-P., Langevin, Y., Gondet, B., et al. (2005). Olivine and pyroxene diversity in the crust of Mars. *Science*, *307*(5715), 1594–1597. https://doi.org/10.1126/science.1109098

Mustard, J. F., Murchie, S. L., Pelkey, S. M., Ehlmann, B. L., Milliken, R. E., Grant, J. A., et al. (2008). Hydrated silicate minerals on Mars observed by the Mars Reconnaissance Orbiter CRISM instrument. *Nature*, *454*(7202), 305–309. https://doi.org/10.1038/nature07097

Navrotsky, A., Mazeina, L., & Majzlan, J. (2008). Size-driven structural and thermodynamic complexity in iron oxides. *Science*, *319*(5870), 1635–1638. https://doi.org/10.1126/science.1148614

Nemchin, A. A., Humayun, M., Whitehouse, M. J., Hewins, R. H., Lorand, J.-P., Kennedy, A., et al. (2014). Record of the ancient Martian hydrosphere and atmosphere preserved in zircon from a Martian meteorite. *Nature Geoscience*, *7*(9), 638–642. https://doi.org/10.1038/ngeo2231

Nesbitt, H. W., & Muir, I. J. (1988). SIMS depth profiles of weathered plagioclase and processes affecting dissolved Al and Si in some acidic soil solutions. *Nature*, *334*(6180), 336–338. https://doi.org/10.1038/334336a0

Neubeck, A., Duc, N. T., Hellevang, H., Oze, C., Bastviken, D., Bacsik, Z., & Holm, N. G. (2014). Olivine alteration and H2 production in carbonate-rich, low temperature aqueous environments. *Planetary and Space Science*, *96*, 51–61. https://doi.org/10.1016/j.pss.2014.02.014

Niles, P. B., Catling, D. C., Berger, G., Chassefière, E., Ehlmann, B. L., Michalski, J. R., et al. (2013). Geochemistry of carbonates on Mars: Implications for climate history and nature of aqueous environments. *Space Science Reviews*, *174*(1-4), 301–328. https://doi.org/10.1007/s11214-012-9940-y

Nugent, M. A., Brantley, S. L., Pantano, C. G., & Maurice, P. A. (1998). The influence of natural mineral coatings on feldspar weathering. *Nature*, *395*(6702), 588–591. https://doi.org/10.1038/26951

Oelkers, E. H., & Schott, J. (2009). *Thermodynamics and kinetics of water-rock interaction*, *Mineralogical Society of America; Geochemical Society*, (Vol. 70).

Parkhurst, D. L., & Appelo, C. A. J. (2013). Description of input and examples for PHREEQC version 3—A computer program for speciation, batch-reaction, one-dimensional transport, and inverse geochemical calculations. *U.S. Geological Survey Techniques and Methods*, available only at http://pubs.usgs.gov/tm/06/a 43/.

Peretyazhko, T. S., Niles, P. B., Sutter, B., Morris, R. V., Agresti, D. G., Le, L., & Ming, D. W. (2018). Smectite formation in the presence of sulfuric acid: Implications for acidic smectite formation on early Mars. *Geochimica et Cosmochimica Acta*, *220*, 248–260. https://doi.org/10.1016/j.gca.2017.10.004

Peretyazhko, T. S., Sutter, B., Morris, R. V., Agresti, D. G., Le, L., & Ming, D. W. (2016). Fe/Mg smectite formation under acidic conditions on early Mars. *Geochimica et Cosmochimica Acta*, *173*, 37–49. https://doi.org/10.1016/j.gca.2015.10.012

Pokrovsky, O. S., & Schott, J. (2000). Kinetics and mechanism of forsterite dissolution at 25°C and pH from 1 to 12. *Geochimica et Cosmochimica Acta*, *64*(19), 3313–3325. https://doi.org/10.1016/S0016-7037(00)00434-8

Poulet, F., Beaty, D. W., Bibring, J.-P., Bish, D., Bishop, J. L., Noe Dobrea, E., et al. (2009). Key Scientific Questions and Key Investigations from the FirstInternational Conference on Martian Phyllosilicates. *Astrobiology*, *9*(3), 257–267. https://doi.org/10.1089/ast.2009.0335

Poulet, F., Bibring, J.-P., Mustard, J. F., Gendrin, A., Mangold, N., Langevin, Y., et al. (2005). Phyllosilicates on Mars and implications for early Martian climate. *Nature*, *438*(7068), 623–627. https://doi.org/10.1038/nature04274

Poulet, F., Mangold, N., Loizeau, D., Bibring, J.-P., Langevin, Y., Michalski, J., & Gondet, B. (2008). Abundance of minerals in the phyllosilicate-rich units on Mars. *Astronomy & Astrophysics*, *487*(2), L41–L44. https://doi.org/10.1051/0004-6361:200810150

Proskurowski, G., Lilley, M. D., Seewald, J. S., Fruh-Green, G. L., Olson, E. J., Lupton, J. E., et al. (2008). Abiogenic hydrocarbon production at Lost City hydrothermal field. *Science*, *319*(5863), 604–607. https://doi.org/10.1126/science.1151194

Putnis, A. (2014). Why mineral interfaces matter. *Science*, *343*(6178), 1441–1442. https://doi.org/10.1126/science.1250884

Rampe, E. B., Ming, D. W., Blake, D. F., Bristow, T. F., Chipera, S. J., Grotzinger, J. P., et al. (2017). Mineralogy of an ancient lacustrine mudstone succession from the Murray formation, Gale crater, Mars. *Earth and Planetary Science Letters*, *471*, 172–185. https://doi.org/10.1016/j.epsl.2017.04.021

Roach, L. H., Mustard, J. F., Swayze, G., Milliken, R. E., Bishop, J. L., Murchie, S. L., & Lichtenberg, K. (2010). Hydrated mineral stratigraphy of Ius Chasma, Valles Marineris. *Icarus*, *206*(1), 253–268. https://doi.org/10.1016/j.icarus.2009.09.003

Ruiz-Agudo, E., King, H. E., Patiño-López, L. D., Putnis, C. V., Geisler, T., Rodriguez-Navarro, C., & Putnis, A. (2016). Control of silicate weathering by interface-coupled dissolution-precipitation processes at the mineral-solution interface. *Geology*, *44*(7), 567–570. https://doi.org/10.1130/G37856.1

Ruiz-Agudo, E., Putnis, C. V., Rodriguez-Navarro, C., & Putnis, A. (2012). Mechanism of leached layer formation during chemical weathering of silicate minerals. *Geology*, *40*(10), 947–950. https://doi.org/10.1130/G33339.1

Sautter, V., Toplis, M. J., Wiens, R. C., Cousin, A., Fabre, C., Gasnault, O., et al. (2015). In situ evidence for continental crust on early Mars. *Nature Geoscience*, *8*(8), 605–609. https://doi.org/10.1038/ngeo2474

Schott, J., Berner, R. A., & Sjöberg, E. L. (1981). Mechanism of pyroxene and amphibole weathering—I. Experimental studies of iron-free minerals. *Geochimica et Cosmochimica Acta*, *45*(11), 2123–2135. https://doi.org/10.1016/0016-7037(81)90065-X

Schröder, C., Klingelhöfer, G., & Tremel, W. (2004). Weathering of Fe-bearing minerals under Martian conditions, investigated by Mössbauer spectroscopy. *Planetary and Space Science*, *52*(11), 997–1010. https://doi.org/10.1016/j.pss.2004.07.018

Sholes, S. F., Smith, M. L., Claire, M. W., Zahnle, K. J., & Catling, D. C. (2017). Anoxic atmospheres on Mars driven by volcanism: Implications for past environments and life. *Icarus*, *290*, 46–62. https://doi.org/10.1016/j.icarus.2017.02.022

Sutter, B., McAdam, A. C., Mahaffy, P. R., Ming, D. W., Edgett, K. S., Rampe, E. B., et al. (2017). Evolved gas analyses of sedimentary rocks and eolian sediment in Gale Crater, Mars: Results of the Curiosity rover's sample analysis at Mars instrument from Yellowknife Bay to the Namib Dune. *Journal of Geophysical Research: Planets*, *122*, 2574–2609. https://doi.org/10.1002/2016JE005225

Taylor, S. R., & McLennan, S. M. (2009). *Planetary crusts*. Cambridge.

Tosca, N. J., Knoll, A. H., & McLennan, S. M. (2008). Water activity and the challenge for life on early Mars. *Science*, *320*(5880), 1204–1207. https://doi.org/10.1126/science.1155432

Tosca, N. J., McLennan, S. M., Lindsley, D. H., & Schoonen, M. A. A. (2004). Acid-sulfate weathering of synthetic Martian basalt: The acid fog model revisited. *Journal of Geophysical Research*, *109*, E05003. https://doi.org/10.1029/2003JE002218

Turner, S. M. R., Bridges, J. C., Grebby, S., & Ehlmann, B. L. (2016). Hydrothermal activity recorded in post Noachian-aged impact craters on Mars. *Journal of Geophysical Research: Planets*, *121*, 608–625. https://doi.org/10.1002/2015JE004989

Vaniman, D. T., Bish, D. L., Ming, D. W., Bristow, T. F., Morris, R. V., Blake, D. F., et al. (2014). Mineralogy of a mudstone at Yellowknife Bay, Gale crater, Mars. *Science*, *343*(6169). https://doi.org/10.1126/science.1243480

Velde, B., & Meunier, A. (2008). *The origin of clay minerals in soils and weathered rocks*. Berlin Heidelberg: (Spinger). https://doi.org/10.1007/978-3-540-75634-7

Wittmann, A., Korotev, R. L., Jolliff, B. L., Irving, A. J., Moser, D. E., Barker, I., & Rumble, D. (2015). Petrography and composition of Martian regolith breccia meteorite Northwest Africa 7475. *Meteoritics & Planetary Science*, *50*(2), 326–352. https://doi.org/10.1111/maps.12425

Wollast, R. (1967). Kinetics of the alteration of K-feldspar in buffered solutions at low temperature. *Geochimica et Cosmochimica Acta*, *31*(4), 635–648. https://doi.org/10.1016/0016-7037(67)90040-3

Wray, J. J., Murchie, S. L., Bishop, J. L., Ehlmann, B. L., Milliken, R. E., Wilhelm, M. B., et al. (2016). Orbital evidence for more widespread carbonate-bearing rocks on Mars. *Journal of Geophysical Research: Planets*, *121*, 652–677. https://doi.org/10.1002/2015JE004972

Zhu, C., Veblen, D. R., Blum, A. E., & Chipera, S. J. (2006). Naturally weathered feldspar surfaces in the Navajo Sandstone aquifer, Black Mesa, Arizona: Electron microscopic characterization. *Geochimica et Cosmochimica Acta*, *70*(18), 4600–4616. https://doi.org/10.1016/j.gca.2006.07.013

Zolotov, M. Y., & Mironenko, M. V. (2016). Chemical models for Martian weathering profiles: Insights into formation of layered phyllosilicate and sulfate deposits. *Icarus*, *275*, 203–220. https://doi.org/10.1016/j.icarus.2016.04.011